Supplementary Information (SI) for Journal of Materials Chemistry A.

Supporting information

Zeolitic Imidazolate Frameworks Enhanced Conductive Nanocomposite Hydrogels with High Stretchability and Low Hysteresis for Self-Powered Multifunctional Sensors

Jishuai Xu[a], Jingye Liang[a], Jingxuan Zheng[a], Fangying Lu[a], Yilian Ma[b], Hanbing Yu[a], Weiqiang Zhao[*b], Run Wang[*a], Zunfeng Liu[b]

[a]School of Textile Science and Engineering, Tiangong university, 399 West Binshui Road, Tianjin 300387, China.

E-mail: wangrun@tiangong.edu.cn

[b]State Key Laboratory of Medicinal Chemical Biology, key Laboratory of Functional Polymer Materials, College of Chemistry Frontiers Science Center for New Organic Matter, Nankai University, 94 Weijin Road, Tianjin 300071, China.

E-mail: zhaoweiqiang@nankai.edu.cn

Experimental Section

Materials

Zinc acetate, 2-methylimidazole (Hmim,98%), methanol, acrylamide (Am), polyvinylpyrrolidone (PVP), N,N′-Methylene-bis-acrylamide (MBAA), and 2-hydroxy-4′-(2-hydroxyethoxy)-2-methylpropiophenone (I-2959) were purchased from Aladdin (Shanghai) Co., Ltd. Sodium chloride (NaCl) were purchased from Macklin (Shanghai) Co., Ltd. Deionized water was used in the experiment (18.2 MΩ·cm resistivity at 20.0°C).

Synthesis of ZIF-8 Nanoparticles

ZIF-8 nanoparticles were synthesized following a previously reported method[1]. Specifically, 3.2 g Hmim and 0.9 g zinc acetate were separately dissolved in 100.0 mL of methanol. Then, the above two solutions were mixed and stirred at room temperature for 3 h. The resulting solid product was collected by centrifugation at 8000 rpm for 10 min, washed three times with methanol, and freeze-dried for 24 h before use.

Preparation of ZIF-8@PAm/PVP hydrogel

First, 0.6 g of NaCl was dissolved in 10 mL of deionized water. Next, 6.0 g of Am monomer and 0.6 g of PVP (10.0 wt% relative to the monomer mass) were added and stirred at room temperature until completely dissolved. Subsequently, 5.0 mg of crosslinking agent MBAA, and 10.0 mg of photoinitiator I-2959, ZIF-8 nanoparticles at different concentrations (relative to the monomer mass) were added to the solution. The mixture was then poured into a polytetrafluoroethylene mold and irradiated under UV light (365 nm) for 40 min to form ZIF-8@PAm/PVP hydrogel. The brittle first network, PAM chain, served as a sacrificial bond to dissipate energy significantly via internal fracture. The interpenetrated ductile second network, PVP chain, was responsible for bearing large deformations. Its flexibility and elasticity contributed to the high stretchability of the hydrogel, enabling it to withstand significant mechanical strain without breaking. NaCl provided ionic conductivity and the anti-freezing properties, allowing the hydrogel to maintain its functionality at low temperatures. ZIF-

8 acted as a physical crosslinker within the hydrogel. It strengthened the network structure by forming additional crosslinking points, thereby improving the mechanical properties and stability of the hydrogel.

Characterization

The microstructure of the ZIF-8 nanoparticles and hydrogels was observed using Cold Field-Emission Scanning Electron Microscopy (FE-SEM, Hitachi S4800, Japan) at voltage of 10.0 kV. The attenuated total reflection Fourier-transform infrared spectroscopy of hydrogels was conducted using a spectrometer (Nicolet iS50, Thermo Fisher) in the range of 500 to 4000 cm^{-1}. The transparency of hydrogels was characterized using an ultraviolet and visible spectrophotometer (UV-Vis) in the range of 200-800 nm (UH4150, Hitachi, Japan). X-ray diffraction (XRD) was performed using a D8 DISCOVER diffractometer (Germany) with Mo Kα radiation, operating at 40.0 kV and 30.0 mA, over a 2θ range of 5.0-60.0°. Differential scanning calorimetry (DSC) analysis was conducted using a 200F3 DSC instrument (Germany) with a heating rate of 5 K min^{-1} from -80.0°C to 20.0°C under a nitrogen atmosphere. A modular compact rheometer (MCR302, Austria) was used to measure the storage modulus (G') and loss modulus (G'') of the hydrogels. In the course of angular frequency scanning measurements, the frequency was varied from 0.01 to 100 rad s^{-1} at a strain of 1%.

Water Retention

The water retention ability of the ZIF-8@PAm/PVP hydrogel tested by the weighing method with different time at humidity of 40.0% and 20.0°C. The weight ratio was defined as

$$\text{Weight ratio (\%)} = M_{\mathrm{i}} - M_0 \tag{1}$$

where M_i and M_0 represent the hydrogel mass at different times and the initial mass, respectively.

Mechanical measurement

Mechanical tests were performed on a Universal Tensile Testing Machine (HY0580, Heng Yi, China). Unless otherwise stated, a hydrogel sample with 30.0 × 7.0× 0.7 mm (length × width × thickness) was used for the tensile testing at a temperature of 20.0^{o}C and humidity of 40.0%, with a deformation rate of 10 mm min^{-1}. The loading-unloading curve was employed to evaluate the dissipative energy and hysteresis of the hydrogel. The dissipative energy (ΔE) was defined as the area enclosed by the loading-unloading process, calculated by the following formula:

$$\Delta E = \left(\int \sigma d\varepsilon\right)_{Loading} - \left(\int \sigma d\varepsilon\right)_{Unloading} \tag{2}$$

The hysteresis was defined by the Equation as the following formula:

$$Hysteresis = \Delta E / \left(\int \sigma d\varepsilon\right)_{Loading} \tag{3}$$

where σ and ε represent tensile stress and strain, respectively.

The tensile stress (σ) of hydrogels was defined by the Equation as the following formula:

$$\sigma = \frac{F}{A} \tag{4}$$

where F was the load force recorded by the universal machine and A was the cross-section area of hydrogels.

The tensile strain (ε) of the hydrogel was defined by the Equation as the following formula:

$$\varepsilon = \frac{l - l_0}{l_0} \times 100\% \tag{5}$$

where l_0 was the initial length of hydrogels between the fixtures and l was the length of hydrogels before breakage.

Electrical measurement

The electrochemical workstation (CHI660E, Shanghai) was used to measure the electrochemical impedance spectroscopy of the hydrogel strain sensor, with a frequency range of 1.0 Hz to 1000.0 Hz. and a voltage of 100.0 mV. Unless otherwise stated, the hydrogel strain sensor with 30.0 × 7.0 × 0.7 mm (length × width × thickness) was used for the electrical testing at a temperature of 20.0°C and humidity of 40.0%.

The electrical resistance during the strain sensing was tested by connecting a nickel-plated copper sheet (7.0 mm x 7.0 mm rectangle) as an electrode to both ends of the hydrogel strain sensor to an LCR tester (IM3536). The LCR tester recorded the resistance signal of the hydrogel strain sensor during deformation, where the applied voltage was 1.0 V and the frequency was 800.0 Hz. The formula for calculating electrical conductivity (σ_e, S/m) was as follows:

$$\sigma_e = L/(R_0 * A) \tag{6}$$

Where L represented the length of the specimen, R_0 denoted the initial resistance, and A stranded for the cross-sectional area of the specimen. The relative resistance change ($\Delta R/R_0$) and Gauge factor (*GF*) were used to evaluate the sensing performance of the hydrogel strain sensor. The calculation formula was as follows:

$$\Delta R/R_0 = (R_s - R_0)/R_0 \tag{7}$$

$$GF = ({}^{\Delta R}/{}_{R_0})/\varepsilon \tag{8}$$

where R_0 represented the original resistance before the application of strain, R_s represented the real-time resistance during the application of strain, and ε represented the strain.

Fabrication and characterization of the triboelectric nanogenerator

The conductive hydrogel (25.0 mm × 25.0 mm × 1.0 mm) was attached with a copper tape as current collector. Then, two pieces of silicone elastomer (thickness of 1.0 mm) was fabricated by mixing component A and component B of Ecoflex in 1:1 weight ratio and curing the complex in a mold at 50.0°C for 3 h. After peel off the Ecoflex layer from the mold, the hydrogel was sealed by the prepared elastomer with the assistance of the uncured elastomer. After curing the device at room temperature for 24 h, the hydrogel based single-electrode triboelectric nanogenerator (TENG) was obtained. The changes in the electrical signal of hydrogel-based TENG were recorded by Keithley 6517.

All human body related experiments of wearable devices on a volunteer were performed in compliance with the relevant laws and institutional guidelines and under approval from Tiangong University. All participants were giving informed consent before participating in the study.

Supporting Figures

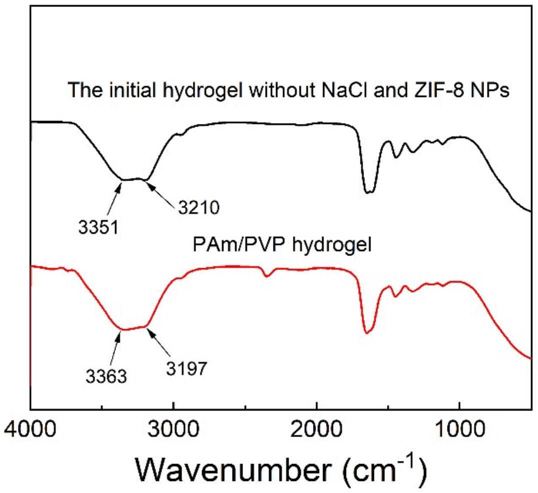

Fig. S1 Fourier-transform infrared spectroscopy of the initial hydrogel without NaCl and ZIF-8 NPs and PAm/PVP hydrogel.

Fig. S2 The ZIF-8@PAm/PVP hydrogel on human skins.

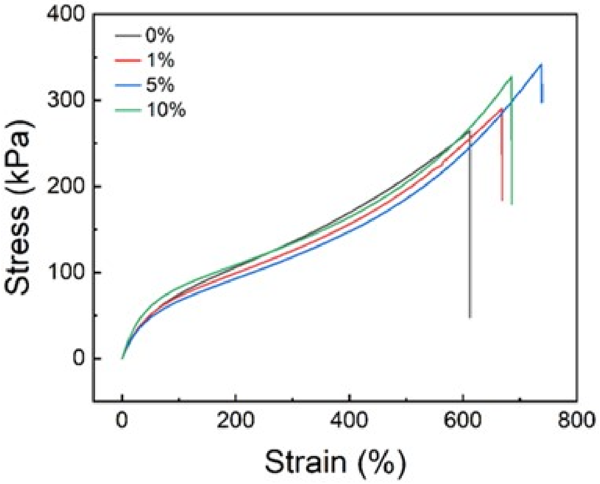

Fig. S3 Typical stress-strain curves of PAm/PVP hydrogels with different content of NaCl.

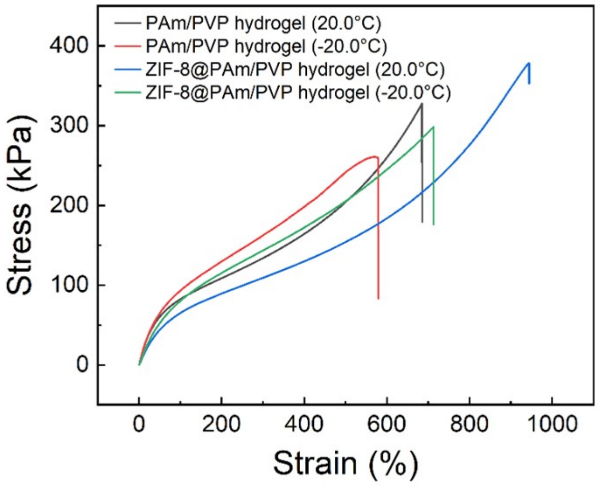

Fig. S4 Typical stress-strain curves of ZIF-8@PAm/PVP hydrogels at different temperature.

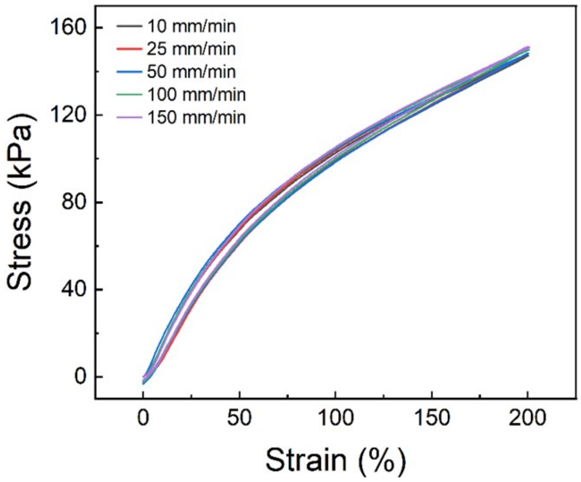

Fig. S5 Stress-recovery curves of ZIF-8@PAm/PVP hydrogel dependence on different strain rates.

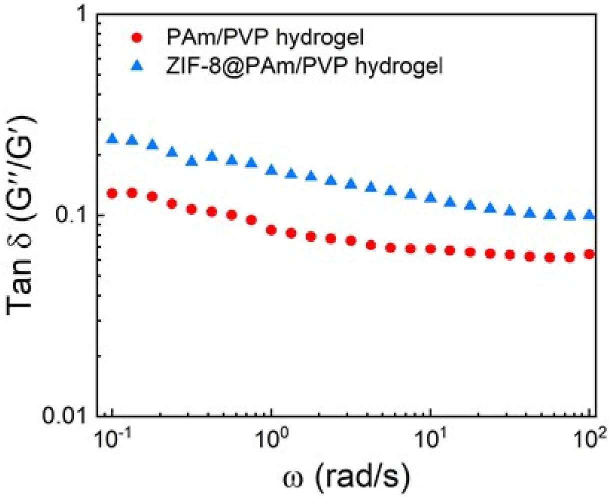

Fig. S6 The tan δ (G''/G') of PAm/PVP hydrogel and ZIF-8@PAm/PVP hydrogel based on the dynamic rheological results under a frequency sweep from 0.1 to 100.0 rad s^{-1}.

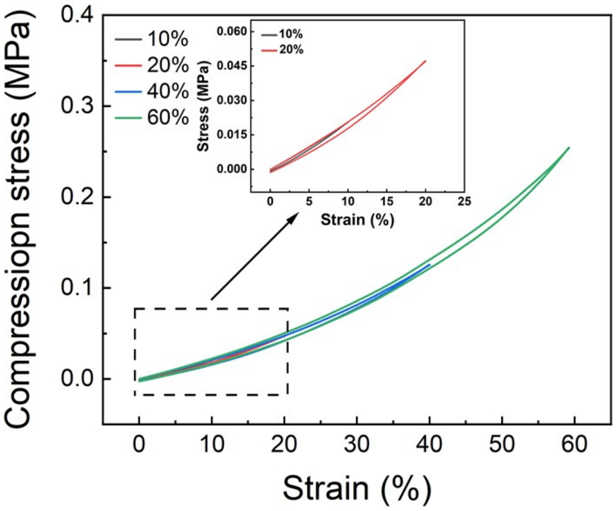

Fig. S7 Stress-recovery curves of ZIF-8@PAm/PVP hydrogel under different compression strains.

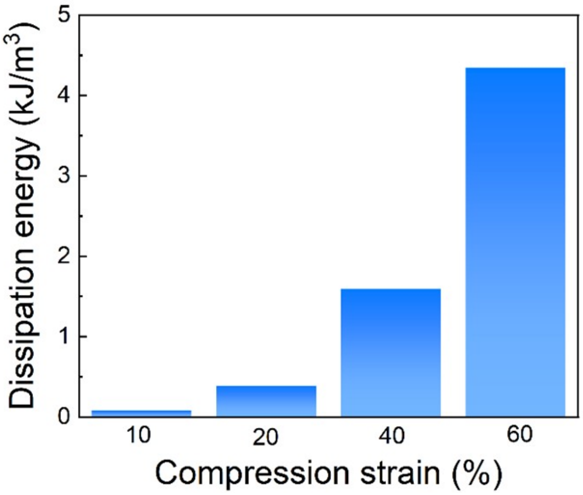

Fig. S8 The dissipation energy of ZIF-8@PAm/PVP hydrogel under different compression strains.

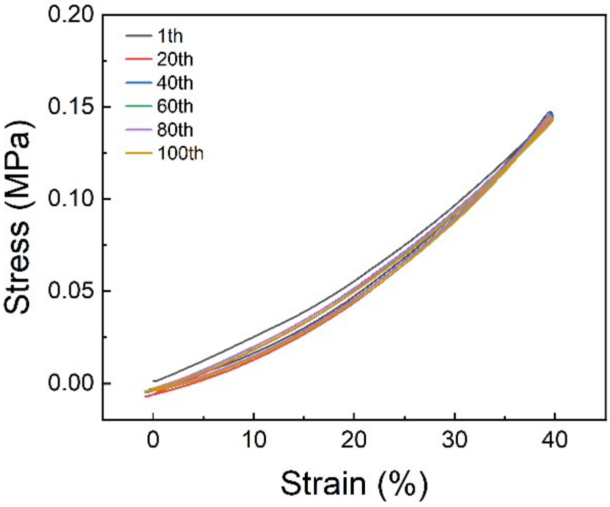

Fig. S9 Cyclic compression test of ZIF-8@PAm/PVP hydrogel under compression at the range of 0-40.0% over 100 cycles.

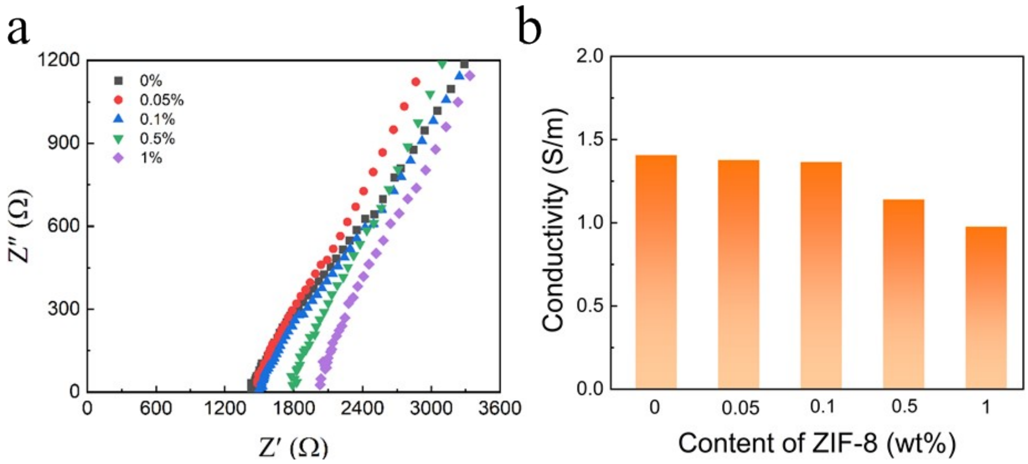

Fig. S10 (a) Electrochemical impedance spectroscopy Nyquist plots and (b) corresponding ionic conductivity of ZIF-8@PAm/PVP hydrogels with different content of ZIF-8 NPs.

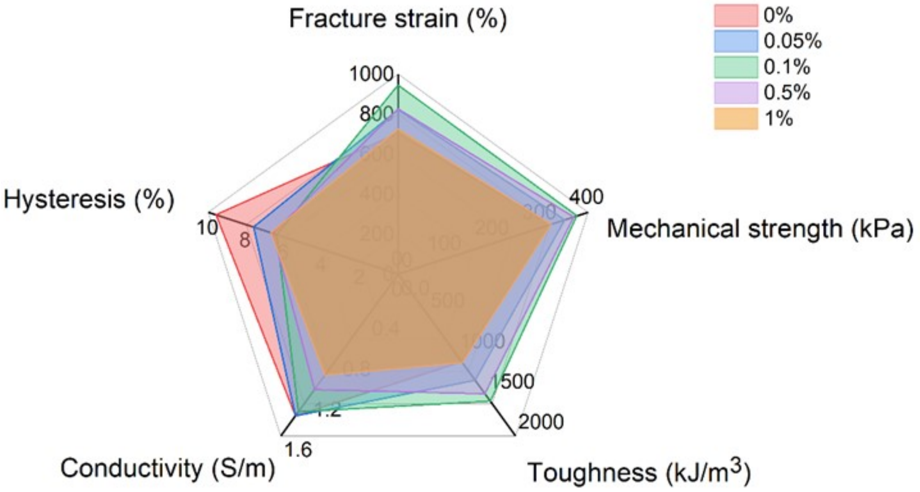

Fig. S11 Comparison of ZIF-8@PAm/PVP hydrogels with different contents of ZIF-8 NPs in terms of mechanical strength, fracture strain, hysteresis, toughness, and conductivity.

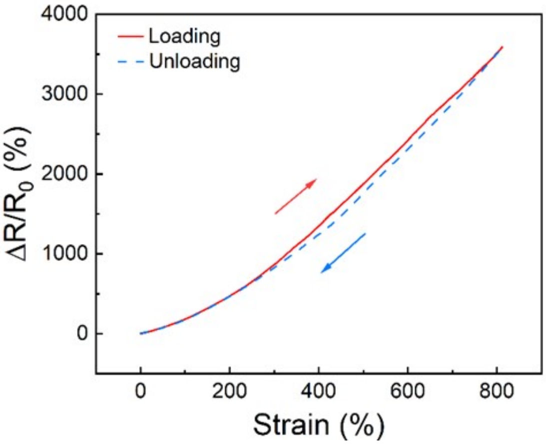

Fig. S12. Relative resistance changes of the hydrogel sensor under 800.0% strain during loading-unloading cycles.

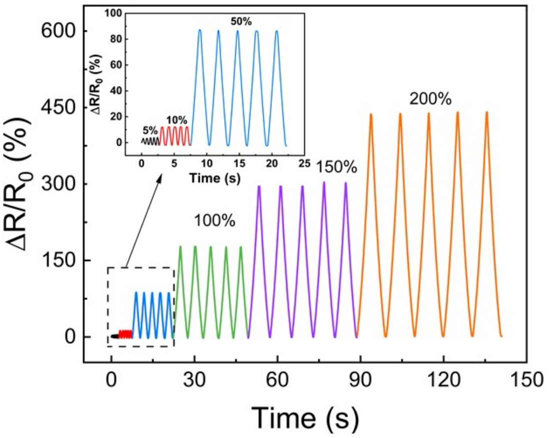

Fig. S13 The cyclic relative resistance changes of the hydrogel strain sensor under different strains.

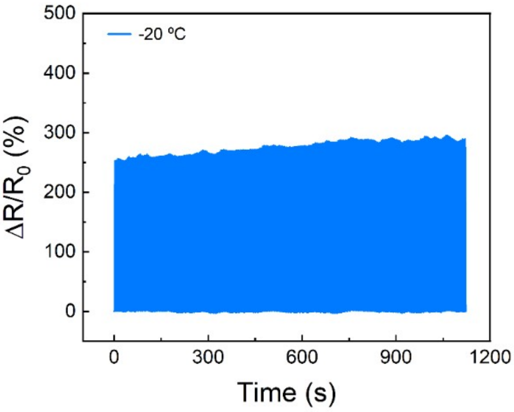

Fig. S14 The cyclic relative resistance changes of the hydrogel sensor at low temperatures.

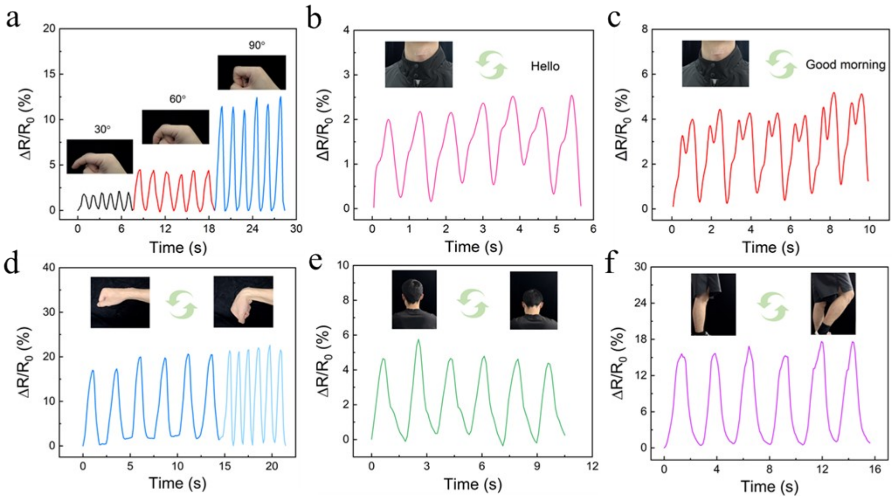

Fig. S15 Real-time relative resistance changes of the hydrogel strain sensors for monitoring the human movements. (a) Finger bending at different angles. (b and c) Saying "Hello" and "Good morning". (d) Wrist bending at different speeds. (e and f) Neck and knee bending.

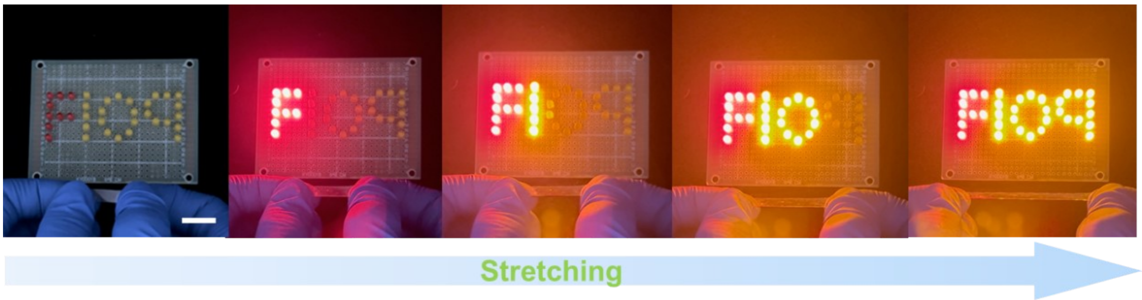

Fig. S16 The hydrogel strain sensor was integrated with programming and additional hardware to manipulate LED.

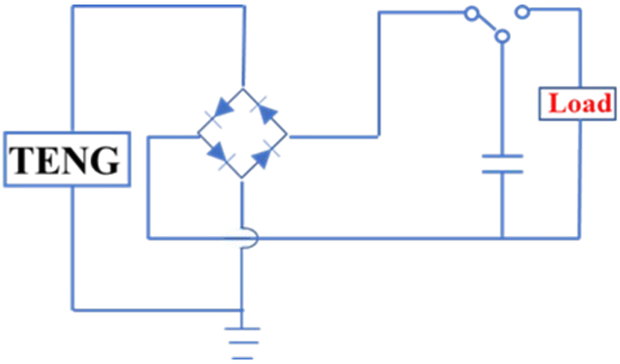

Fig. S17 Equivalent circuit of capacitor charging of the hydrogel-based TENG with capacitors.

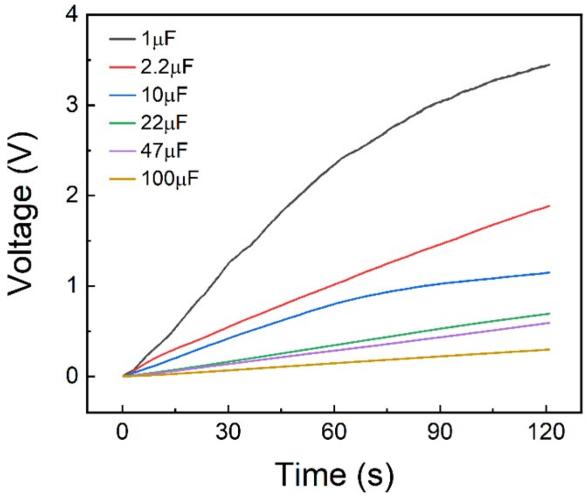

Fig. S18 The TENG of charging capability was demonstrated by charging a series of commercial capacitors at 3.0 Hz.

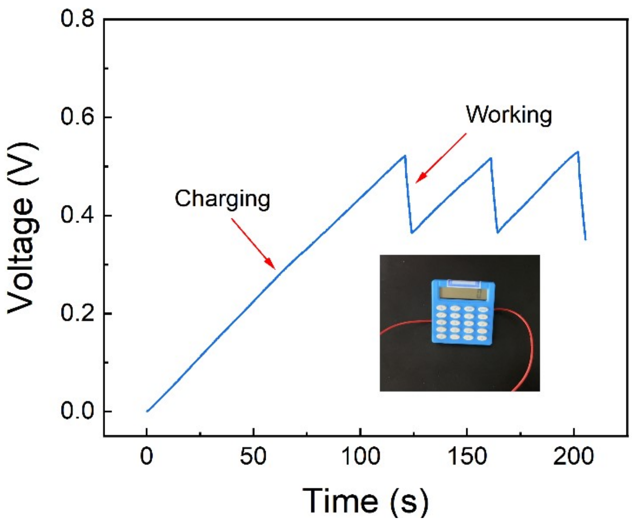

Fig. S19 The TENG was transduced into direct current through the bridge rectifier to charge the capacitor.

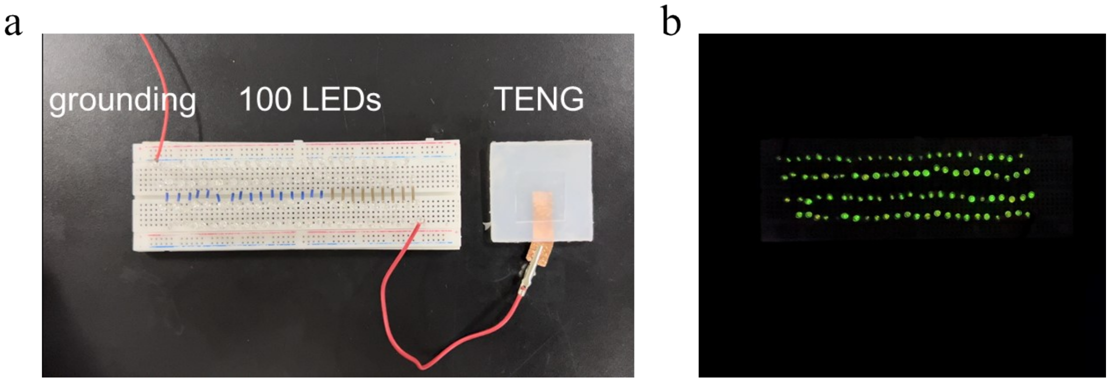

Fig. S20 (a) The circuit diagram of the TENG connected to 100LEDs. (b) Digital showing the 100 LEDs lighting.

Supporting Tables

Summary of performance results of reported conductive hydrogel

Table S1. Summary of performance results of reported conductive hydrogel

Conductive component	Tensile strain (%)	Hysteresis (%)	Freeze tolerance	Ref
LiCl	500.0	12.00	Yes	2
Ionic liquid	550.0	7.00	No	3
PEDOT:PSS	300.0	1.50	No	4
MXene	500.0	3.00	No	5
LiCl	200.0	3.00	No	6
Ionic liquid	500.0	9.00	No	7
Silica nanoparticles	600.0	1.30	No	8
NaCl	200.0	5.00	No	9
AMPS	500.0	21.39	No	10
NaCl	800.0	6.50	Yes	This work

Table S2 Summary of performance results of reported conductive hydrogel

Conductive component	Tensile strain (%)	Gauge factor (%)	Freeze tolerance	Ref
Laponite	750.0	2.68	Yes	11
LiCl	250.0	1.24	No	6
Ionic liquid	300.0	6.54	No	12
$AlCl_3$	350.0	2.84	Yes	13
PANI nanoparticles	200.0	2.43	Yes	14
MXene	500.0	2.23	No	15
NaCl	600.0	0.81	Yes	16
MXene	350.0	5.98	No	17
Silica nanoparticles	500.0	5.86	No	18
NaCl	900.0	6.38	Yes	This work

Supporting Videos

Supporting video S1: A demonstration of the activation and deactivation of the LED can be manipulated by the hydrogel strain sensor.

Supporting video S2: A demonstration of the calculator was powered using a capacitor charged from the hydrogel based TENG.

Supporting video S3: A demonstration of the hydrogel based TENG for mechanical energy harvesting to turn-on and turn-off of 100 LEDs.

References

1. T. Zhu, S. Xu, F. Yu, X. Yu and Y. Wang, *Journal of Membrane Science*, 2020, **598**, 117681.
2. H. Wang, B. Liu, D. Chen, Z. Wang, H. Wang, S. Bao, P. Zhang, J. Yang and W. Liu, *Materials Horizons*, 2024, **11**, 2628-2642.
3. R. Du, T. Bao, T. Zhu, J. Zhang, X. Huang, Q. Jin, M. Xin, L. Pan, Q. Zhang and X. Jia, *Advanced Functional Materials*, 2023, **33**, 2212888.
4. Z. Shen, Z. Zhang, N. Zhang, J. Li, P. Zhou, F. Hu, Y. Rong, B. Lu and G. Gu, *Advanced Materials*, 2022, **34**, 2203650.
5. Y. Liu, G. Tian, Y. Du, P. Shi, N. Li, Y. Li, Z. Qin, T. Jiao and X. He, *Advanced Functional Materials*, 2024, **34**, 2315813.
6. J. Liu, X. Chen, B. Sun, H. Guo, Y. Guo, S. Zhang, R. Tao, Q. Yang and J. Tang, *Journal of Materials Chemistry A*, 2022, **10**, 25564-25574.
7. S. Han, Y. Hu, J. Wei, S. Li, P. Yang, H. Mi, C. Liu and C. Shen, *Advanced Functional Materials*, 2024, **34**, 2401607.
8. X. Meng, Y. Qiao, C. Do, W. Bras, C. He, Y. Ke, T. Russell and D. Qiu, *Advanced Materials*, 2022, **34**, 2108243.
9. T. Li, X. Li, J. Yang, H. Sun and J. Sun, *Advanced Materials*, 2023, **35**, 2307990.
10. G. Chen, O. Hu, J. Lu, J. Gu, K. Chen, J. Huang, L. Hou and X. Jiang, *Chemical Engineering Journal*, 2021, **425**, 131505.
11. J. Zou, X. Jing, Z. Chen, S. Wang, X. Hu, P. Feng and Y. Liu, *Advanced Functional Materials*, 2023, **33**, 2213895.
12. F. Hu, Z. Huang, C. Luo and K. Yue, *Materials Horizons*, 2023, **10**, 5907-5919.
13. J. Wen, J. Tang, H. Ning, N. Hu, Y. Zhu, Y. Gong, C. Xu, Q. Zhao, X. Jiang, X. Hu, L. Lei, D. Wu and T. Huang, *Advanced Functional Materials*, 2021, **31**, 2011176.
14. X. Yu, H. Zhang, Y. Wang, X. Fan, Z. Li, X. Zhang and T. Liu, *Advanced Functional Materials*, 2022, **32**, 2204366.
15. M. Wang, L. Li and T. Zhang, *Nano Energy*, 2024, **126**, 109586.
16. Y. Long, B. Jiang, T. Huang, Y. Liu, J. Niu, Z. L. Wang and W. Hu, *Advanced Functional Materials*, 2023, **33**, 2304625.
17. J. Zou, X. Jing, S. Li, P. Feng, Y. Chen and Y. Liu, *Small*, 2024, **20**, 2401622.
18. X. Yu, Y. Zheng, H. Zhang, Y. Wang, X. Fan and T. Liu, *Chemistry of Materials*, 2021, **33**, 6146-6157.